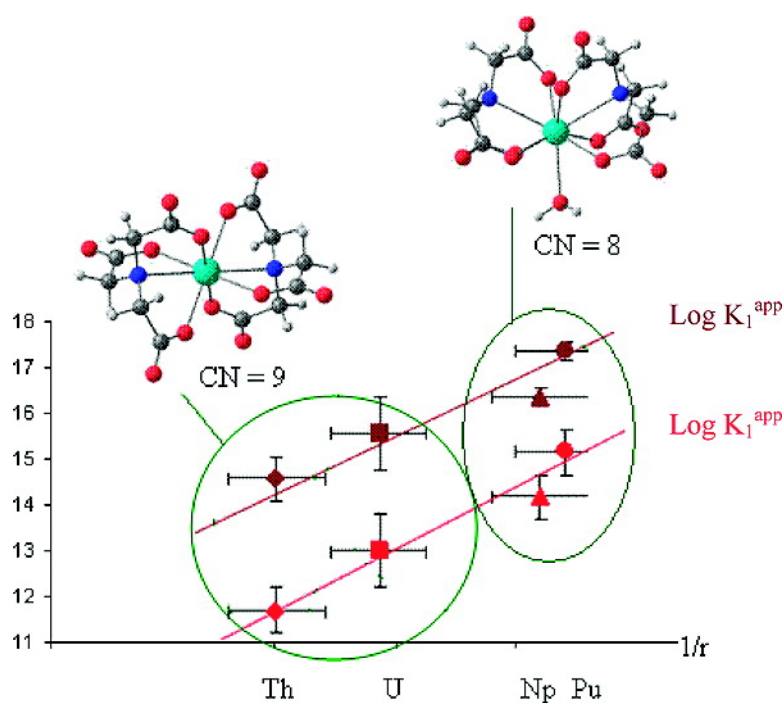Article

Thermodynamics and Structure of Actinide(IV) Complexes with Nitrilotriacetic Acid

L. Bonin, D. Guillaumont, A. Jeanson, C. Den Auwer, M. Grigoriev, J.-C. Berthet, C. Hennig, A. Scheinost, and Ph. Moisy

More About This Article

Additional resources and features associated with this article are available within the HTML version:

- Supporting Information
- Access to high resolution figures
- Links to articles and content related to this article
- Copyright permission to reproduce figures and/or text from this article

View the Full Text HTML

Inorganic Chemistry
Article

Thermodynamics and Structure of Actinide(IV) Complexes with Nitrilotriacetic Acid

L. Bonin,[†] D. Guillaumont,[†] A. Jeanson,[†] C. Den Auwer,[†] M. Grigoriev,[‡] J.-C. Berthet,[§] C. Hennig,[||] A. Scheinost,[||] and Ph. Moisy*,[†]

CEA Marcoule, DEN/DRCP/SCPS, BP 17171, 30207 Bagnols sur Ceze, France, A. N. Frumkin Institute of Physical Chemistry and Electrochemistry, RAS, Leninskii Prosp. 31, 119991 Moscow, Russia, CEA Saclay, DSM, IRAMIS, Service de Chimie Moléculaire, CNRS URA 331, 91191 Gif-sur-Yvette, France, and Forschungszentrum Dresden-Rossendorf, Institute of Radiochemistry, D 01314 Dresden, Germany

Nitrilotriacetic acid, commonly known as NTA ($N(CH_2CO_2H)_3$), can be considered a representative of the polyaminocarboxylic family. The results presented in this paper describe the thermodynamical complexation and structural investigation of An(IV) complexes with NTA in aqueous solution. In the first part, the stability constants of the An(IV) complexes (An = Pu, Np, U, and Th) have been determined by spectrophotometry. In the second part, the coordination spheres of the actinide cation in these complexes have been described using extended X-ray absorption fine structure spectroscopy and compared to the solid-state structure of $(Hpy)_2[U(NTA)_2] \cdot (H_2O)$. These data are further compared to quantum chemical calculations, and their evolution across the actinide series is discussed. In particular, an interpretation of the role of the nitrogen atom in the coordination mode is proposed. These results are considered to be model behavior of polyaminocarboxylic ligands such as diethylenetriamine pentaacetic acid, which is nowadays the best candidate for a chelating agent in the framework of actinide decorporation for the human body.

1. Introduction

Polyaminocarboxylates form a promising family of chelating agents of metal ions. They are particularly considered to trap actinide cations in solution, offering perspectives of applications in many areas such as decorporation in human detoxicological processes, synergistic agents in selective extraction processes, and so forth. For instance, diethylenetriamine pentaacetic acid and ethylenediaminetetraacetic acid are attractive molecules in actinide decorporation since in vivo studies have demonstrated their efficiency in the elimination of radioelements when accidentally incorporated in the body. However, despite drawing strong interest, their chemical behavior in the presence of An^{4+} ions (An = actinide) is not completely understood to date. The chemical data, which can been found in the literature, are sparse and often not in accordance. In the present study, nitrilotriacetic acid (NTA) has been considered as a simple model of polyaminocarboxylic acids because of its three identical carboxylic functions and one tertiary amine, which can all act as coordinating groups.

This article is divided into two parts. In the first part, the complexation of the tetravalent actinide ions with NTA has been investigated from a thermodynamical point of view. In the second part, the structure of the complexes in solution and in the solid state is discussed and compared to quantum chemical data.

Much thermodynamics data can be found in the literature concerning the complexation of Th(IV),[1−4] Np(IV),[5] and

* To whom correspondence should be addressed. E-mail: philippe.moisy@cea.fr.
† CEA Marcoule.
‡ A. N. Frumkin Institute of Physical Chemistry and Electrochemistry.
§ CEA Saclay.
|| Forschungszentrum Dresden-Rossendorf.

(1) Courtney, R. C.; Gustafson, R. L.; Chaberek, S., Jr.; Martell, A. E. *J. Am. Chem. Soc.* **1958**, *80*, 2121–2128.
(2) Bogucki, R. F.; Martell, A. E. *J. Am. Chem. Soc.* **1968**, *90*, 6022–6027.
(3) Skorik, N. A.; Kumok, V. N.; Serebrennikov, V. V. *Russ. J. Inorg. Chem.* **1967**, *12*, 1788–1790.
(4) Bottari, E.; Anderegg, G. *Helv. Chim. Acta* **1967**, *50*, 2349–2356.
(5) Eberle, S. H.; Paul, M. Th. *J. Inorg. Nucl. Chem.* **1971**, *33*, 3067–3075.

Pu(IV)[6] with nitrilotriacetic acid in aqueous media. In particular, the stability constants of the complexes have been determined in several studies. For Th(IV), the stability constant of Th^{IV}−NTA has been reported with log K_1 equal to 16.9,[4] 12.4,[1] and 13.25.[3] Two values are on the same order of magnitude, but one value is significantly higher by more than 4 units of log K. For Np(IV) and Pu(IV), the following values have been reported in the literature: log $K_1 = 17.28$ and log $K_2 = 14.78$[5] for Np(IV) and log $K_1 = 12.86$[6] for Pu(IV). However, it is very unlikely that the stability constants are lower for Pu(IV) than for Np(IV). Therefore, there is a strong lack of coherency in the reported data, and more coherent and accurate data along the actinide series are needed.

Structural investigations of metallic complexes with NTA have been the subject of numerous studies in the solid state.[7] Tetravalent and trivalent metal ions tend to form oligomeric and polymeric structures, but crystal structures of monomeric 1:2 complexes have also been described. The M^{4+} ions (M = Zr, Sn, Hf, and Hg)[8] generally form eight-coordinate M(NTA)$_2$ complexes where the metal ion is coordinated by six carboxylic oxygen atoms and two nitrogen atoms. With the trivalent M^{3+} ions (M = Y,[7] Bi,[9] In,[10] lanthanides[11]), the complexes can be eight- (6 + 2) or nine- (6 + 3) coordinate. In some studies, Wang et al. have described the various coordinating modes of NTA. In all of the cases, the three carboxylic oxygen and nitrogen atoms interact with the metal center. In the case of the oxophilic lanthanides, the Ln^{3+} ion often retains water in its first coordination sphere, as in K$_3$[Nd(NTA)$_2$(H$_2$O)]·6H$_2$O[12] or [Pr(NTA)-(H$_2$O)$_2$]·H$_2$O.[13] In the latter case, NTA is a tetradentate ligand coordinating one of the Pr^{3+} ions with the nitrogen atom and three oxygen atoms of the carboxylic groups and coordinating the second Pr^{3+} with one oxygen atom from the same carboxylic group, which acts as a bridging ligand. In [Nd(NTA)(H$_2$O)]$_n$, each of the three carboxylic groups of the same NTA molecule are bridging between the two Nd^{3+} cations.[14] This demonstrates the versatility of the NTA ligand, which can behave either as a tetradentate chelate or as a single to triply bridging ligand. The sizes of the lanthanide cations also play a key role, as the coordination number tends to decrease from nine for Pr to eight for Yb.[13]

In solution, structural data have been obtained from vibrational, fluorescence, nuclear magnetic resonance, and X-ray absorption spectroscopy for M^{3+} ions with NTA.[15−18] From these studies, different binding modes have been proposed where NTA may act as a tridentate or a tetradentate ligand with or without metal−nitrogen bonds. To our knowledge, no detailed structural studies of actinide(IV)−NTA complexes in solution or in the solid state have been reported to date.

In the present work, the formation of 1:1 and 1:2 complexes in aqueous solution is described for An^{4+} cations (An = Th, U, Np, Pu), and the corresponding stability constants have been determined. These results have been obtained from spectrophotometric measurements, with a variation either of the acidity [H$^+$] or of the molar quantity of NTA. Moreover, the structures in solution of the 1:2 complexes have been investigated using extended X-ray absorption fine structure (EXAFS) at the actinide L$_{III}$ edge for Th(IV), U(IV), Np(IV), and Pu(IV) cations. Comparison with the solid-state structure of (Hpy)$_2$[U(NTA)$_2$]·(H$_2$O) (1·H$_2$O) obtained from single-crystal diffraction data is also provided. In addition, quantum chemical calculations are a unique tool for investigating variations in the coordination sphere across a series of analogous complexes. In this work, such calculations have fostered discussion about the relative stability of several conformations and coordination modes in light of both thermodynamics and structural data. The role of the nitrogen atom of NTA with regard to its interaction with the metal cation is also discussed.

2. Experimental Section

2.1. Chemical Preparation. 2.1.1. Stock Solutions. Reagent-grade 36% HCl and 67% HNO$_3$ (Prolabo) were used to fit the acidity. Hydroxylammonium nitrate (6 M) and chloride were used to reduce Np(V) to Np(IV); they were prepared from a stock solution of 50% NH$_2$OH (Fluka) and HNO$_3$ or HCl. Hydrazinium nitrate (HN = N$_2$H$_5$NO$_3$; 1 M) was used to prevent the formation of nitrous acid and was prepared by the addition of HNO$_3$ to hydrazinium hydroxide (Merck). Nitrilotriacetic acid solutions of various concentrations were prepared by dissolution of commercially available solid H$_3$NTA (Prolabo) in acidic media. By adjusting the acidity from 0.1 to 5 M with HNO$_3$ or HCl, various NTA buffers with a [NTA]$_{tot}$ from 10^{-4} M to 0.01 M were prepared. Dilutions were carried out with distillate water (18 M Ω·cm) obtained through a ELGASTAT UHQ MKII purifier.

Actinide (U, Np, and Pu) was obtained from the CEA inventory. Most of the An^{IV}−NTA samples were prepared through a mixture of the stock solution with various quantities of chelating solutions. The low acidity was controlled by adding HNO$_3$ or HCl fractions to avoid a pH > 1, which would induce hydrolysis of An(IV).

(6) Nitsche, H.; Becraft, K. *Transuranium Elements: A Half Century, 200th ACS National Meeting (August 1990)*; American Chemical Society: Washington, DC, 1992; Chapter 29, pp 276−287.

(7) Allen, F. H. *Acta Crystallogr.* **2002**, *B58*, 380−388.

(8) (a) Logvinova, V. B.; Davidovich, R. L.; Ilyukhin, A. B.; Sergienko, V. S.; Tkachev, V. V.; Atovmyan, L. O. *Koord. Khim.* **1998**, *24*, 568. (b) Davidovich, R. L.; Samsonova, I. N.; Teplukhina, L. V.; Shchelokov, R. N. *Russ. J. Coord. Chem.* **1997**, *23*, 327−329.

(9) Stavila, V.; Davidovich, R. L.; Gulea, A.; Whitmire, K. H. *Coord. Chem. Rev.* **2006**, *250*, 2782−2810.

(10) Sysoeva, T. F.; Starikova, Z. A.; Ershova, S. D.; Dyatlova, N. M. *Zh. Strukt. Khim.* **1991**, *32*, 163.

(11) Kang, J. G.; Kang, H. J.; Jung, J. S.; Yun, S. S.; Kim, C. H. *Bull. Korean Chem. Soc.* **2004**, *25*, 852−858.

(12) Wang, J.; Zhang, X. D.; Ling, X.; Jia, W. G.; Li, H. F. *J. Mol. Struct.* **2002**, *610*, 151−158.

(13) Wang, J.; Zhang, X. D.; Zhang, Y.; Jia, W. G.; Liu, Zh. R. *J. Struct. Chem.* **2004**, *45*, 114−123.

(14) Haung, L.; Zhang, Li.-P.; Jin Lin, P. *J. Mol. Struct.* **2004**, *692*, 121−126.

(15) Kilyen, M.; Lakatos, A.; Latajka, R.; Labadi, I.; Salifoglou, A.; Raptopoulou, C. P.; Kozlowski, H.; Kiss, T. *J. Chem. Soc., Dalton Trans.* **2002**, *18*, 3578−3586.

(16) Asato, E.; Kamamuta, K.; Imade, R.; Yamasaki, M. *Inorg. React. Mech. (Philadelphia, PA, U. S.)* **2000**, *2*, 57−68.

(17) Babushkina, T. A.; Kovaleva, E. V.; Klimova, T. P.; Zemnukhova, L. A.; Krainova, N. Y. *Russ. J. Coord. Chem.* **2004**, *30*, 555−558.

(18) Mathur, J. N.; Thakur, P.; Dodge, C. J.; Francis, A. J.; Choppin, G. R. *Inorg. Chem.* **2006**, *45*, 8026−8035.

A stock solution of Pu(IV), obtained after purification of Pu(IV) by ion exchange on an anionic resin, AGMP1 (DOWEX), was diluted to obtain a 3.15×10^{-2} M stock solution of Pu(IV) (0.95 M HNO_3).

Neptunium was purified also on an anionic resin, and then it was precipitated at the V oxidation state as $Np^{V}O_2OH \cdot xH_2O$ ($x \sim$ 2.5). Stock solutions of Np(V) were prepared in an acidic medium (HNO_3 and HCl) by dissolving a known mass of $Np^{V}O_2OH \cdot xH_2O$ (M = 331 g/mol). Np(IV) stock solutions, 5×10^{-2} M in hydrochloric acid and 2×10^{-2} M in nitric acid, were prepared by reducing a Np^{V} solution with hydroxylammonium chloride or nitrate, in an acidic medium at 70 °C (in the presence of HN to prevent the formation of HNO_2 and the oxidation of Np(IV) in nitric acid media). The reduction of neptunium from Np(V) to Np(IV) was followed spectrophotometrically, with less than 1% Np(V) in the HCl solution and less than 5% in the HNO_3 solution.

A stock solution of 0.48 M U(IV) in 1.1 M HNO_3, with 0.15 M HN obtained by catalytic hydrogenation, was diluted to obtain a 4.8×10^{-2} M stock solution in a HNO_3 medium (0.5 M), in the presence of hydrazinium nitrate (0.1 M HN) to prevent the formation of HNO_2 and the oxidation of U(IV).

Solid thorium nitrate ($Th(NO_3)_4 \cdot 5H_2O$; Prolabo) was used as received.

2.1.2. Synthesis of (Hpy)$_2$[U(NTA)$_2$] (1). Manipulations of the uranium(IV) compounds were carried out under argon (<5 ppm oxygen or water) using standard Schlenk-vessel and vacuum-line techniques or using a glovebox. Pyridine (Aldrich) was dried over KH and distilled immediately before use. Dimethylformamide (Aldrich) was stored under argon over 3 Å molecular sieves. The nitrilotriacetic acid (H_3NTA, Fluka) was dried under a vacuum at room temperature for 1 h and stored under argon. Though sparingly soluble at room temperature, the H_3NTA readily dissolves in refluxing pyridine. Elemental analyses were performed by Analytische Laboratorien at Lindlar (Germany). UCl_4[19] and $U(Otf)_4$[20] were prepared as previously described.

A flask was charged with UCl_4 (103 mg, 0.271 mmol) and H_3NTA (105.2 mg, 0.550 mmol), and pyridine (20 mL) was condensed at −70 °C. After 30 min of stirring at 60 °C, a green deposit was formed, and the solution was pale yellow in color. In order to ensure complete reaction, the suspension was then further warmed at 95 °C for 12 h. The green insoluble was then filtered off, washed with hot pyridine (3 × 10 mL), and dried under a vacuum for 48 h at 25 °C to afford an analytically pure pale-green powder (1). Yield: 95% (200 mg). Anal. calcd for $C_{22}H_{24}N_4O_{12}U$: C, 34.12; H, 3.12; N, 7.23. Found: C, 33.96; H, 3.05; N, 7.18. Complex **1** is too insoluble in pyridine-d_5 to derive a ^1H NMR spectrum.

Pale-green needles of the water solvate **1·H$_2$O**, suitable for X-ray diffraction analysis, were obtained in a NMR tube, by warming at 130 °C for 24 h the U(IV) triflate complex $U(Otf)_4$ (15 mg, 0.012 mmole) and 2 equiv of H_3NTA (6.9 mg) in a mixture of dimethylformamide (1 mL) and pyridine (0.1 mL).
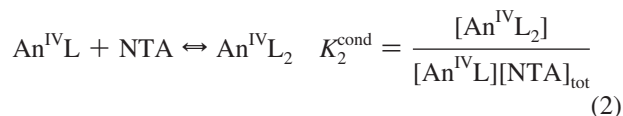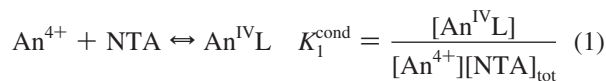
2.1.3. Preparation of the EXAFS Samples. Complexes of An^{IV} with NTA were prepared at neutral pH (6−7). An acidic solution of free An^{IV} (Th, U, Np, or Pu) was first added to solid Na_3NTA, so that $2.5[An^{IV}] < [NTA] < 3[An^{IV}]$, in order to form the An^{IV}−NTA_2 complex. This solution was then diluted in an appropriate buffer (HEPES, 2-[4-(2-hydroxyethyl)-1-piperazine]ethanesulfonic acid; Sigma ≥99.5%) to reach a pH of 6−7.

(19) Hermann, J. A.; Suttle, J. F. *Inorg. Synth.* **1957**, *5*, 143−145.
(20) Berthet, J. C.; Lance, M.; Nierlich, M.; Ephritikhine, M. *Eur. J. Inorg. Chem.* **1999**, *11*, 2005−2007.

Table 1. Characteristics of the Spectra Assigned to the Various An^{IV} Species

	An^{4+}		$An^{IV}L$		$An^{IV}L_2$	
	λ_{max} (nm)	ε	λ_{max} (nm)	ε	λ_{max} (nm)	ε
Pu^{IV}	476	59	487	27	497	19
Np^{IV} (HCl)	723	147	732	119	739	145
Np^{IV} (HNO_3)	723	94	732	109	739	160
U^{IV}	652	33	664	103		

2.2. Spectrophotometric Studies and Equilibrium Measurements. Measurements were carried out on a Schimadzu 3101 spectrophotometer at room temperature, with a 1-cm-path-length quartz cell. The resolution was fixed at 0.5 nm. The evolution of the bands when increasing quantities of ligand (L) were added was followed spectrophotometrically and was used in the determination of the stability constants. Both the total amount of NTA and the acidity of the sample have an influence on the amount of chelation formed. For low ligand concentrations (namely, low quantities of NTA and high acidities >1 M), the addition of NTA results in a decrease of the intensity of the band corresponding to the free An(IV) cation, while a peak appears and increases at a higher wavelength. This band is assigned to the complex, of stoichiometry 1:1, $An^{IV}L$. The known spectrum is subtracted from the experimental ones in order to get a "zero signal" (±0.005 absorption units with respect to the baseline in the wavelength range of interest). The free An(IV) rate in solution can thus be obtained. Consequently, the residue corresponds to the fraction of the first complex. By normalizing the average spectrum corresponding to those residues, the characteristics of the spectrum of $An^{IV}L$ (wavelength and molar extinction coefficient) can be determined. For higher ligand concentrations (namely, higher quantities of NTA and lower acidities <1 M), the addition of NTA results in a decrease of the intensity of the band corresponding to $An^{IV}L$, while a peak appears and increases at a higher wavelength. This band is assigned to the complex, of stoichiometry 1:2, $An^{IV}L_2$. The spectrum of $An^{IV}L$, determined in the preceding step, is subtracted from the experimental ones in order to get a "zero signal". The $An^{IV}L$ rate in solution can thus be obtained. Consequently, the residue corresponds to the fraction of the second complex. By normalizing those residues, the characteristics of the spectrum of $An^{IV}L_2$ (wavelength and molar extinction coefficient) can be determined (Table 1).
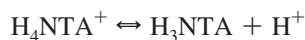
The contribution of free An^{IV}, $An^{IV}L$, and $An^{IV}L_2$ in each sample can thus be determined by deconvolution. This leads to the calculation of the concentration of each species in solution. The conditional stability constants can then be calculated from the following equilibriums:

$$An^{4+} + NTA \leftrightarrow An^{IV}L \quad K_1^{cond} = \frac{[An^{IV}L]}{[An^{4+}][NTA]_{tot}} \quad (1)$$

$$An^{IV}L + NTA \leftrightarrow An^{IV}L_2 \quad K_2^{cond} = \frac{[An^{IV}L_2]}{[An^{IV}L][NTA]_{tot}} \quad (2)$$
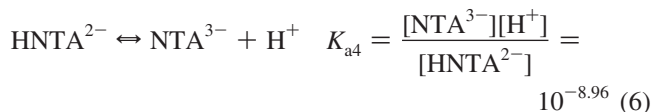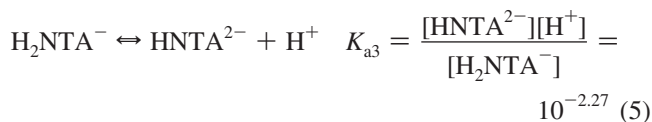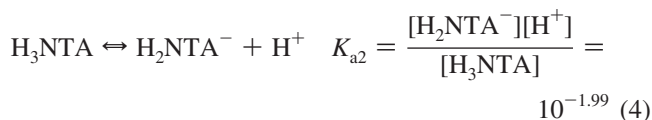
The concentration of the chelating form of NTA (named L) is deduced from the total amount of NTA introduced in each sample and the acidity constants. The N atom is taken into account as being involved in the complexation due to its acid−base properties (pK_{a4}). Several sets of pK_a can be found in the literature for various ionic strengths. They vary considerably depending on the experimental conditions. The following acidity constants for nitrilotriacetic acid at $I = 1$ M are chosen:[5]

$$H_4NTA^+ \leftrightarrow H_3NTA + H^+$$

$$K_{a1} = \frac{[H_3NTA][H^+]}{[H_4NTA^+]} = 10^{-0.8} \quad (3)$$

$$H_3NTA \leftrightarrow H_2NTA^- + H^+ \quad K_{a2} = \frac{[H_2NTA^-][H^+]}{[H_3NTA]} = 10^{-1.99} \quad (4)$$

$$H_2NTA^- \leftrightarrow HNTA^{2-} + H^+ \quad K_{a3} = \frac{[HNTA^{2-}][H^+]}{[H_2NTA^-]} = 10^{-2.27} \quad (5)$$

$$HNTA^{2-} \leftrightarrow NTA^{3-} + H^+ \quad K_{a4} = \frac{[NTA^{3-}][H^+]}{[HNTA^{2-}]} = 10^{-8.96} \quad (6)$$

knowing that, at the equilibrium,

$$[NTA]_{tot} = [H_4NTA^+] + [H_3NTA] + [H_2NTA^-] + [HNTA^{2-}] + [NTA^{3-}] + [An^{IV}L] + 2[An^{IV}L_2]$$
$$= \alpha[L] + [An^{IV}L] + 2[An^{IV}L_2] \quad (7)$$

$$[L] = \frac{[NTA]_{tot} - [An^{IV}L] - 2[An^{IV}L_2]}{\alpha} \quad (8)$$

As [L] is considered to be the most basic form of NTA,

$$\alpha = 1 + 10^{pK_{a4}}[H^+] + 10^{pK_{a4}+pK_{a3}}[H^+]^2 + 10^{pK_{a4}+pK_{a3}+pK_{a2}}[H^+]^3 + 10^{pK_{a4}+pK_{a3}+pK_{a2}+pK_{a1}}[H^+]^4 \quad (9)$$

Knowing α, which depends only on the acidity, the apparent stability constants can be calculated:

$$K_1^{app} = \frac{[An^{IV}L]}{[An^{4+}][L]} \quad (10)$$

$$K_2^{app} = \frac{[An^{IV}L_2]}{[An^{IV}L][L]} \quad (11)$$

$$\beta_2^{app} = \frac{[An^{IV}L_2]}{[An^{4+}][L]^2} \quad (12)$$

In contrast to An^{IV}, Th^{IV} cannot be directly followed by spectrophotometry. A means to determine its behavior is to study how Th^{IV} competes with another An^{IV} ion in its complexation with NTA. Due to the poor spectral resolution and the difficulty of the spectrum deconvolution, U^{IV} is not considered, and the experiments are carried out with Np^{IV}, whose spectra can more easily be followed. Knowing the stability constants of Np^{IV}, different solutions of Np and NTA of known composition are prepared in nitric acid, with only two species in solution: Np^{4+} and NpL.

Various quantities of solid thorium nitrate are added in each sample, up to Np/Th = 1:100.

Np and Th compete to form complexes with NTA:

$$Np^{4+} + L \rightarrow Np^{IV}L \quad K_{1,Np} \quad (13)$$

$$Th^{4+} + L \rightarrow Th^{IV}L \quad K_{1,Th} \quad (14)$$

The absorption spectra of the samples are measured by spectrophotometry. Knowing the stability constants of $Np^{IV}L$, and being able to determine the rate [free Np^{IV}]/[$Np^{IV}L$] or [$Np^{IV}L$]/[$Np^{IV}L_2$] from the spectra, the amount of the free chelating form of NTA in each solution can be calculated from eqs 15 and 16:

$$[L] = \frac{[Np^{IV}L]}{K_1^{Np}[Np^{4+}]} \quad (15)$$

$$[L] = \frac{[Np^{IV}L_2]}{K_2^{Np}[Np^{IV}L]} \quad (16)$$

Moreover, this quantity of ligand is also given by

$$[L] = \frac{[NTA]_{tot} - [Np^{IV}L] - 2[Np^{IV}L_2] - [Th^{IV}L] - 2[Th^{IV}L_2]}{\alpha} \quad (17)$$

The initial solution was prepared in such a way that there was no $Np^{IV}L_2$ in solution. It can be assumed that there is no $Th^{IV}L_2$ complex formed either in solution, as far as the chelation of NTA with Th(IV) should be weaker than with Np(IV).

This leads to [L] = ([NTA]$_{tot}$ − [Np^{IV}L] − [Th^{IV}L])/α and thus to [Th^{IV}L]. When the total amount of Th^{IV} introduced in each sample is known, the ratio [Th^{IV}L]/[Th^{4+}] is easily deduced, and so is the stability constant $K_1^{Th} = [Th^{IV}L]/([Th^{4+}][L])$.

2.3. Crystallographic Data Collection and Structure Determination. The data were collected at 100(2) K on a Nonius Kappa-CCD area detector diffractometer[21] using graphite-monochromated Mo Kα radiation ($\lambda = 0.71073$ Å). The crystals were placed inside glass capillaries with a protecting "Paratone-N" oil (Hampton Research) coating. The unit cell parameters were determined from 10 frames and then refined on all data. A 180° φ range was scanned with 2° steps during data collection. The data were processed with DENZO-SMN.[22] The structures were solved by Patterson map interpretation with SHELXS-97 and subsequent Fourier-difference synthesis and refined by full-matrix least squares on F^2 with SHELXL-97.[23] Absorption effects were corrected empirically with the program MULABS from PLATON.[24] All non-hydrogen atoms were refined with anisotropic displacement parameters. Hydrogen atoms of NTA and Hpy were introduced at calculated positions and were treated as riding atoms with displacement parameters equal to 1.2 times the U_{eq} values of the parent atoms. Hydrogen atoms of the crystallization water molecule were not located. The molecular plots were drawn with SHELXTL.[25]

Crystal data for **1**·H$_2$O: (Hpy)$_2$[U(NTA)$_2$]·(H$_2$O), C$_{22}$H$_{26}$N$_4$O$_{13}$U, $M = 792.50$, orthorhombic, space group *Pbca* (no. 61), $a = 22.6935(8)$ Å, $b = 9.4783(3)$ Å, $c = 23.9262(9)$ Å, $V = 5146.4(3)$ Å^3, $Z = 8$, $T = 100(2)$ K, μ(Mo Kα) = 6.384 mm^{-1}. A total of 29 244 reflections and 4484 unique reflections ($R_{int} = 0.067$) were

(21) *Kappa-CCD Software*; Nonius BV: Delft, The Netherlands, 1998.
(22) Otwinowski, Z.; Minor, W. Methods in Enzymology. *Macromolecular Crystallography, Part A*; Carter, C. W., Jr., Sweet, R. M., Eds.; Elsevier: New York, 1997; Vol. 276, pp 307−326.
(23) Sheldrick, G. M. *SHELXS97; SHELXL97*; University of Göttingen: Göttingen, Germany, 1997.
(24) Spek, A. L. *PLATON*; University of Utrecht: Utrecht, The Netherlands, 2000.
(25) Sheldrick, G. M. *SHELXTL*, version 5.1; Bruker AXS Inc.: Madison, WI, 1999.

measured, which were used in all calculations. The final $R(F)$ and $wR(F^2)$ were 0.0417 and 0.1028 for 3723 reflections with $I > 2\sigma(I)$ and 0.0531 and 0.1080 for all data; the goodness of fit was 1.101.

2.4. EXAFS Data Acquisition and Data Treatment. EXAFS measurements were performed in 200 μL cells specifically designed for radioactive samples. To avoid oxidation of U(IV) by the atmosphere, the uranium sample was maintained under argon before the experiment and aluminum windows instead of kapton windows were used for the EXAFS cells. EXAFS measurements were carried out on the Rossendorf beam line (ROBL)[26] at ESRF (European Synchrotron Radiation Facility) (6.0 GeV at 200 mA) in fluorescence mode, at room temperature, with a Si(111) water-cooled monochromator in the channel cut mode. Two Pt-coated mirrors were used for harmonic rejection. Energy calibration was carried out with a Y foil (17 052 eV at the absorption maximum) and a Zr foil (18 014 eV at the absorption maximum) depending on the actinide cation. All spectra were acquired at the actinide L_{III} edge. Data treatment (AUTOBK normalization) was carried out with the Athena[27] code. Data fitting was carried out with the Artemis[25] code in R space between 1.0 and 3.5 Å for the one-shell fit and the multishell fit without any prior data filtering (Kaiser window between 2 and 11 Å^{-1}). Spectra noise was calculated by back Fourier transformation above 6 Å using the CHEROKEE code.[28] Both the R factor and quality factor were calculated in $k^3\chi(k)$ mode. Phases and amplitudes were calculated using the Feff82[29] code from An(NTA)$_2$(H$_2$O)$_1$ clusters (An = Th, U, Np, Pu) obtained from quantum chemical calculations.

Given the spatial resolution of the EXAFS spectra ($\Delta k = 9$ Å^{-1} and therefore ΔR is around $2\pi/9 = 0.7$ Å), the expected difference of distances between the O and N shells (about 0.3 Å in the quantum chemical model clusters) is not resolvable using the EXAFS technique. Therefore, in a first approach, one shell of neighbors in the single scattering approximation has been used for the fitting procedure. In the second approach, we used a parametrized multishell fitting procedure, as exemplified in ref 30. In this method, the entire coordination sphere of the actinide cation obtained from the model clusters is fitted as a semirigid polyhedron with only four structural parameters. The first parameter, δR_n, adjusts the size of the coordination polyhedron as an isotropic correction to each distance R_n. The three other parameters, u, v, and w, are anisotropic geometrical corrections to account for a slight distortion of the cation polyhedron with respect to the model. They represent a displacement in the three directions of space of the cation position with respect to the model cluster inside its coordination sphere. In this procedure, triple scattering paths were included in the fit with no additional parameters since they were structurally linked to the four above parameters. In summary, the following paths are included in the fit: single scattering paths = 6An–O$_{NTA}$ + 2An–N$_{NTA}$ + 6An–C$_{(carboxylate)}$ + 6An–C$_{(\alpha\ of\ N)}$; triple scattering paths = 6An–O$_{NTA}$–C$_{(carboxylate)}$. Variable parameters in the fit are as follows: u, v, w, δR, Debye–Waller factors σ^2(O$_{NTA}$), σ^2(N$_{NTA}$), σ^2(C$_{carboxylate}$) = σ^2(C$_{\alpha\ of\ N}$), and σ^2(triple scat).

2.5. Quantum Chemical Calculations. The geometries of 1:2 complexes were optimized at the DFT level of theory with the

Amsterdam Density Functional (ADF) program package.[31−33] Relativistic effects were considered through the zeroth-order regular approximation (ZORA).[34] Spin−orbit effects were not taken into account. For open-shell systems, the unrestricted DFT method was employed. Uncontracted triple-ζ Slater-type valence orbitals with one set of polarization functions were used for all atoms. The frozen-core approximation was used, where the core density was obtained from four-component Dirac−Slater calculations on all of the atoms and kept frozen during molecular calculations. The 1s^2 core electrons were frozen for carbon, nitrogen, and oxygen. The valence space of the heavy elements includes 6s, 6p, 6d, 5f, and 7s shells of actinides. The density functional consists of a local density part using the parametrization of Vosko, Wilk, and Nusair and exchange-correlation gradient corrected parts of Becke.

Geometries were optimized taking into account aqueous solvation effects. Solvation effects were carried out using a dielectric model where the solute is embedded in a molecular-shaped cavity surrounded by a dielectric medium. The conductor-like solvation model (COSMO) as implemented in the ADF package was used.[35,36] Since solvation effects calculated through a continuum approach depend sensitively on the choice of the molecular-shaped cavity, two different sets of ionic radii were used for O, N, C, and H atoms to construct the cavity. One set corresponds to the radii determined by Stefanovich and Truong[37] and the other set to Klamt radii.[36] For actinides, no radii were found in the literature, and they were determined in order to reproduce hydration energies of actinides(IV). The cavity was constructed as a solvent-excluding surface.

Additional calculations were performed in the gas phase using RECP-based calculations performed with the Gaussian 03 package, in order to calculate analytically vibrational frequencies to ensure that the optimized structures are true minima (with no imaginary frequencies). Energy-adjusted RECPs developed in the Stuttgart/ Cologne group were used together with the accompanying basis set to describe the valence electron density. Small-core RECPs replace 60 core electrons for actinides. The corresponding valence basis sets associated with small-core pseudopotentials are (14s 13p 10d 8f) contracted to [10s 9p 5d 4f] for actinides. A 6-31G* basis set was used for other atoms. Geometries were optimized using the B3LYP functional.

3. Results

3.1. Stability Constants Determination. The chelation of Pu(IV) upon the addition of NTA was followed by spectrophotometry. Absorption maxima and molar extinction coefficients corresponding to the free actinide cation and to complexes with NTA are reported in Table 1. Figure 1 shows the evolution of the absorption band near 476 nm (for free Pu^{IV}) when NTA is added up to 0.01 M, at an acidity of [H$^+$] = 0.5 M. This results in a decrease of the intensity of the peak at 476 nm, while a peak appears with an increasing

(26) Matz, W.; Schell, N.; Bernhard, G.; Prokert, F.; Reich, T.; Clauβner, J.; Oehme, W.; Schlenk, R.; Dienel, S.; Funke, H.; Eichhorn, F.; Betzl, M.; Pröhl, D.; Strauch, U.; Hüttig, G.; Krug, H.; Neumann, W.; Brendler, V.; Reichel, P.; Denecke, M. A.; Nitsche, H. *J. Synchrotron Radiat.* **1999**, *6*, 1076–1085.
(27) Ravel, B.; Newville, M. *J. Synchrotron Radiat.* **2005**, *12*, 537–541.
(28) Michalowicz, A. EXAFS code available at lps2m.univ-paris12.fr/ (accessed Mar 2009).
(29) Rehr, J. J.; Albers, R. C. *Rev. Mod. Phys.* **2000**, *72*, 621–654.
(30) Ruas, A.; Guilbaud, P.; Den Auwer, C.; Moulin, C.; Simonin, J.-P.; Turq, P.; Moisy, P. *J. Phys. Chem. A* **2006**, *110*, 11770–11779.
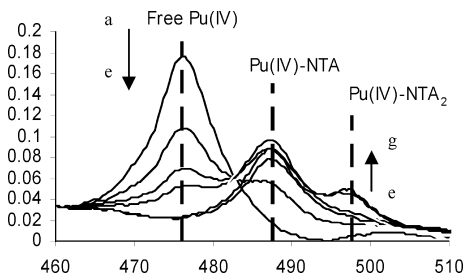
(31) *ADF2006*; Vrije Universiteit: Amsterdam, The Netherlands, 2006. Available at http://www.scm.com (accessed Mar 2009).
(32) te Velde, G.; Bickelhaupt, F. M.; van Gisbergen, S. A. J.; Fonseca Guerra, C.; Baerends, E. J.; Snijders, J. G.; Ziegler, T. *J. Comput. Chem.* **2001**, *931–967.*
(33) Fonseca Guerra, C.; Snijders, J. G.; te Velde, G.; Baerends, E. J. *Theor. Chem. Acc.* **1998**, *99*, 391–403.
(34) van Lenthe, E.; Ehlers, A.; Baerends, E. J. *J. Chem. Phys.* **1999**, *110*, 8943–8953.
(35) Pye, C. C.; Ziegler, T. *Theor. Chem. Acc.* **1999**, *101*, 396–408.
(36) Klamt, A. *J. Phys. Chem.* **1995**, *99*, 2224–2235.
(37) Stefanovich, E. V.; Truong, T. N. *Chem. Phys. Lett.* **1995**, *244*, 65–74.

Figure 1. Evolution of Pu^{IV} spectra with the addition of NTA in nitric acid ($l = 1$ cm, $T = 25$ °C): (a) $[H^+] = 0.5$ M, $[NTA]_{tot} = 0.001$ M; (b) $[H^+] = 0.5$ M, $[NTA]_{tot} = 0.004$ M; (c) $[H^+] = 0.5$ M, $[NTA]_{tot} = 0.006$ M; (d) $[H^+] = 0.5$ M, $[NTA]_{tot} = 0.01$ M; (e) $[H^+] = 0.3$ M, $[NTA]_{tot} = 0.004$ M; (f) $[H^+] = 0.3$ M, $[NTA]_{tot} = 0.008$ M; (g) $[H^+] = 0.3$ M, $[NTA]_{tot} = 0.01$ M.
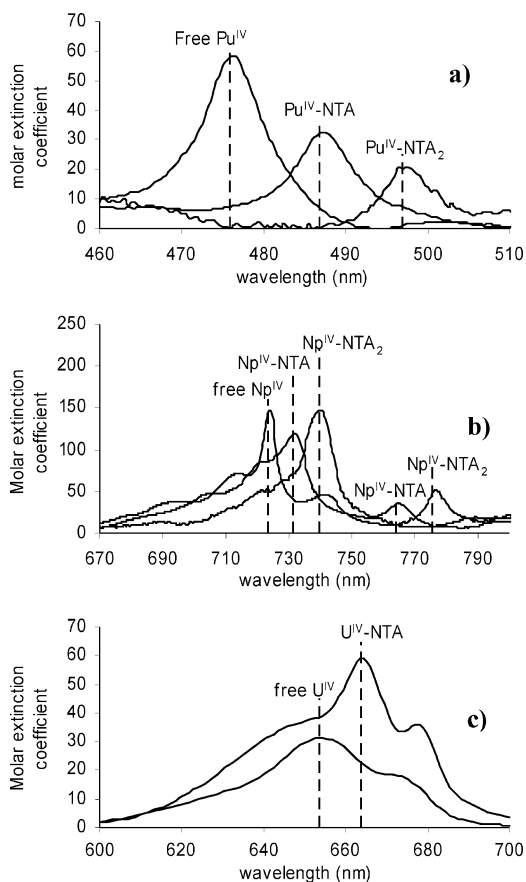
Figure 2. Various spectra for An^{IV} in the presence of NTA: free An^{IV}, $An^{IV}L$, $An^{IV}L_2$ ($l = 1$ cm, $T = 25$ °C). (a) Free Pu^{IV}, $Pu^{IV}L$, and $Pu^{IV}L_2$ in nitric acid medium; (b) free Np^{IV}, $Np^{IV}L$, and $Np^{IV}L_2$ in hydrochloric acid medium; (c) free U^{IV} and $U^{IV}L$ in nitric acid medium.

intensity at 487 nm. This evolution clearly shows the presence of two species in solution: free Pu^{IV} and $Pu^{IV}L$. Lowering the acidity down to $[H^+] = 0.3$ M induces an increase of the concentration of the chelating form of NTA, which leads to a decrease of the peak at 487 nm with a concomitant appearance of a peak at 497 nm with increasing intensity (Figure 1). This evolution demonstrates the existence of the $Pu^{IV}L$ and $Pu^{IV}L_2$ species in solution. The normalized spectra of Pu^{IV}, $Pu^{IV}L$, and $Pu^{IV}L_2$ are shown in Figure 2a (see also Table 1). The deconvolution of the samples' spectra leads to the determination of the apparent stability constants of $Pu^{IV}L$, $\log K_1 = 17.4 \pm 0.2$, and $Pu^{IV}L_2$, $\log K_2 = 15.2 \pm 0.5$ (Table 2).

The same measurements were carried out with Np(IV). The spectrum of free Np^{IV} has a characteristic absorption band near 723.5 nm, at an acidity $[H^+] = 0.5$ M. When NTA is added up to 0.005 M ($[H^+] = 0.5$M), the initial peak decreases, but a new absorption band related to $Np^{IV}L$ appears at 731.5 nm with an increasing intensity. This evolution is related to the presence of two species in solution: free Np^{IV} and $Np^{IV}L$. Lowering the acidity down to $[H^+] = 0.3$ M induces a decrease of the peak at 731.5 nm, while another one corresponding to NpL_2 appears and increases at 739 nm. This evolution suggests the existence of $Np^{IV}L$ and $Np^{IV}L_2$ in solution. The normalized spectra of Np^{IV}, $Np^{IV}L$, and $Np^{IV}L_2$ in a hydrochloric acid medium are shown in Figure 2b (Table 1). The deconvolution of the samples' spectra leads to the determination of the apparent stability constants of $Np^{IV}L$, $\log K_1 = 16.5$, and $Np^{IV}L_2$, $\log K_2 = 14.2$, which are reported in Table 2.

The deconvolution of the samples' spectra obtained in nitric acid with the same methodology leads to the determination of the apparent formation constants of $Np^{IV}L$ and $Np^{IV}L_2$; the values are identical to those obtained in a hydrochloric medium: $\log K_1 = 16.4$ and $\log K_2 = 14.2$ (Table 2).

The distinct spectra of free Np^{IV} in nitric and hydrochloric media show the coordinating influences of the NO_3^- and Cl^- anions, respectively. This medium effect vanishes (or disappears) upon complexation with NTA, and the spectra of the $Np^{IV}L$ and $Np^{IV}L_2$ complexes are identical in both media (Table 1).

The spectrum of the U^{4+} ion solvated in aqueous media exhibits an absorption band at 652 nm. The total concentration of NTA varies from 0 to 0.01 M, at acidities $[H^+] = 0.8, 0.4, 0.2,$ and 0.1 M. At acidities $[H^+] = 0.8$ and 0.4 M, the addition of NTA up to 0.01 M results in a decrease of the band at 652 nm with the appearance of a new peak with an increasing intensity at 664 nm, suggesting the existence of free U^{IV} and $U^{IV}L$. Lowering the acidity down to $[H^+] = 0.2$ or 0.1 M leads to a slight displacement of the $U^{IV}L$ peak. The deconvolution shows that it is due to the apparition of a broad and low-intensity band around 672 nm. This uneasily identified band may be related to the formation of $U^{IV}L_2$. As it partly covers the wavelength range of the two other bands, the determination of the composition of each sample corresponding to each spectrum is most difficult and uncertain. The normalized spectra of U^{IV} and $U^{IV}L$ are shown in Figure 2c. The deconvolution of the samples' spectra leads to the determination of the apparent formation constants of $U^{IV}L$, $\log K_1 = 15.6 \pm 0.8$, and $U^{IV}L_2$, $\log K_2 = 13 \pm 0.8$ (Table 2).

Changes in the spectrum of a solution of $[NpL] = 3[Np^{4+}]$ ($[H^+] = 1$ M, $[Np(IV)]_{Tot} = 2 \times 10^{-3}$ M, $[NTA]_{Tot} = 10^{-2}$ M) by the addition of Th^{4+} are shown in Figure 3. The spectrum exhibits two absorption bands near 723 and 732 nm which are assigned to free Np^{IV} and $Np^{IV}L$, respectively. By increasing the concentration of Th^{IV} (from 0 to 0.22 M), the intensity of the absorption band at 732 nm ($Np^{IV}L$ complex) decreases concomitantly to the increase of the signal of free Np^{IV} at 723 nm. This competition reaction

Table 2. Apparent Stability Constants of Various An^{IV} with NTA

	$\log K_1^{app}$	$\log K_2^{app}$
Th^{IV}	14.6 ± 0.3 ([HNO_3] = 1 M)	11.7 ± 0.8 ([HNO_3] = 1 M)
U^{IV}	15.6 ± 0.8 ([HNO_3] = 0.8 M or 0.4 M)	13 ± 0.8 ([HNO_3] = 0.2 M or 0.1 M)
Np^{IV}	16.4 ± 0.2 ([HNO_3] = 0.5 M)	14.2 ± 0.5 ([HNO_3] = 0.3 M)
	16.5 ± 0.2 ([HCl] = 0.5 M)	14.2 ± 0.5 ([HCl] = 0.3 M)
Pu^{IV}	17.4 ± 0.2 ([HNO_3] = 0.5 M)	15.2 ± 0.5 ([HNO_3] = 0.3 M)

clearly demonstrates the greater stability of $Np^{IV}L$ versus its analogous complex $Th^{IV}L$.

Similar competitive experiments were carried out in order to determine the second stability constant K_2^{Th}. Unfortunately, the achievable conditions cannot allow us to determine this value. Indeed, the equilibrium between NpL and NpL_2, modified by the presence of Th^{IV}, is not significantly affected by the ratio between the various forms of Th, and thus by the formation constant of ThL_2. It can only be estimated that $\log K_2^{Th} < 13$. In order to evaluate more precisely this value, the variation of $\log K_2$ versus $\log K_1$ is represented with our values for An^{IV}–NTA (Figure 4).

For the lanthanides (Ln^{III} from La to Eu), and especially for Ln^{III}–NTA[35] and Ln^{III}–dipicolinate,[38] it can be noticed that $\log K_2 = a \log K_1 + b$, with both ligands. The same evolution is observed for Pu(IV), Np(IV), and U(IV) (Figure 4). It can be assumed that the constants for Th follow this tendency, which leads to the determination of $\log K_2^{Th}$. The resulting value is reported in Table 2.

3.2. Quantum Chemistry Calculations. The structures of An^{IV}–L_2 complexes have been investigated through quantum chemistry calculations. In the present calculations, we have considered eight-coordinate structures corresponding to S_6 and C_2 symmetry (**A** and **B** in Figure 5) and nine-coordinate structures obtained by adding a water molecule in the inner coordination sphere (C_2 symmetry, **C** in Figure 5). Calculated values for actinide–oxygen and actinide–nitrogen bond distances are listed in Table 3 for **A**, **B**, and **C**. The reported values correspond to geometry optimizations
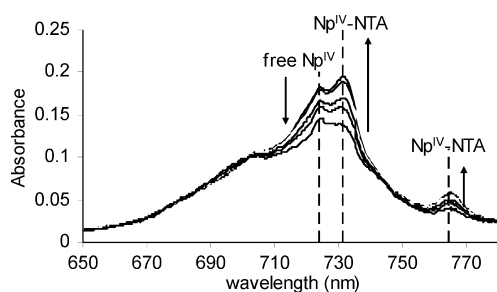
Figure 3. Evolution of the spectrum of Np^{IV}–NTA with the addition of Th^{IV}. $-l = 1$ cm, $T = 25$ °C. [HNO_3] = 1 M, [Np]$_{tot}$ = $2 \cdot 10^{-3}$ M, [NTA]$_{tot}$ = 10^{-2} M, [Th] from 0 to 0.22 M.
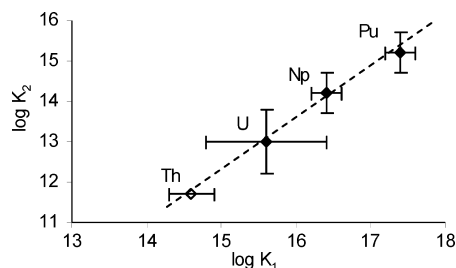
Figure 4. Variation of $\log K_2$ versus $\log K_1$ for An^{IV}–NTA.

using a COSMO model for solvent effects performed at the ZORA/GGA level. Several test calculations using different functionals and basis sets have been performed and have shown that actinide–nitrogen distances vary significantly as a function of the calculation details (within 0.1 Å). Actinide–oxygen bonds are stronger, and their bond distances are much less affected by the calculation approach. However, for both types of distances, the evolution in the series of cations remains similar when varying the calculation method. An–O distances are equal to 2.40–2.41 Å for Th(IV) and are comprised between 2.30 and 2.34 Å for U(IV), Np(IV), and Pu(IV). An–N distances are from 0.3 to 0.4 Å longer than An–O distances. For a given structure, the variations of An–O bond distances as a function of the actinide center follow roughly the evolution of the ionic radii of the cations. From Th(IV) to U(IV), M–O distances get shortened by 0.06, 0.06 and 0.1 Å in **A**, **C**, and **B**, respectively. From U(IV) to Np(IV) and from Np(IV) to Pu(IV), M–O distances decrease from 0.00 to 0.01 Å. The ionic radii diminishes by 0.05 Å from Th^{4+} to U^{4+}, 0.02 Å from U^{4+} to Np^{4+}, and 0.01 Å from Np^{4+} to Pu^{4+}. For all of the cations, a structural change does not imply significant variations in the actinide–oxygen distance; this is not the case for the weaker actinide–nitrogen bonds, which are far more sensitive to the geometry and coordination number.

Energy differences, in solution, of the structures of **A**, **B**, and **C** are given in Table 4. In order to compare the differences in energy of analogous compounds, the energy values have been calculated by considering an additional water molecule in interaction with **A** and **B**. This H_2O molecule is interacting with two carboxylic oxygen atoms through hydrogen bonds but is not coordinated to the actinide cation. Zero-point energy and thermal corrections resulting from translational, rotational, and vibrational motions have not been calculated in solution and are not included in the reported energy values. However, in the gas phase, the difference in the calculated thermal corrections to Gibbs free energy is about 1 kJ mol^{-1} between **A** and **B** and about 4 kJ mol^{-1} between **A** and **C**.

For an eight-coordinate complex, **A** is more stable than **B**, whatever the cations are; the energy difference becomes more important with the diminution of the ionic radius, from 7 kJ mol^{-1} for Th(IV) to 36 kJ mol^{-1} for Pu(IV). The energy
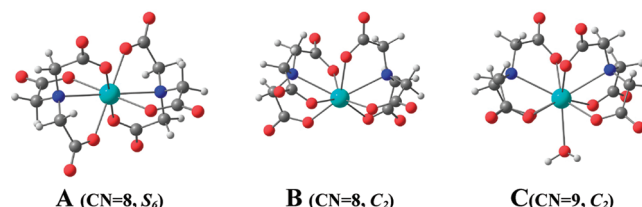
Figure 5. Structures of An^{IV}–NTA_2 complexes.

A (CN=8, S_6)   **B** (CN=8, C_2)   **C** (CN=9, C_2)

Table 3. Calculated An−O and An−N Bond Distances in [An(NTA)$_2$]$^{2-}$ and [An(NTA)$_2$(H$_2$O)]$^{2-}$ Complexes (Mean Values in Å) Corresponding to **A**, **B**, and **C** Structures
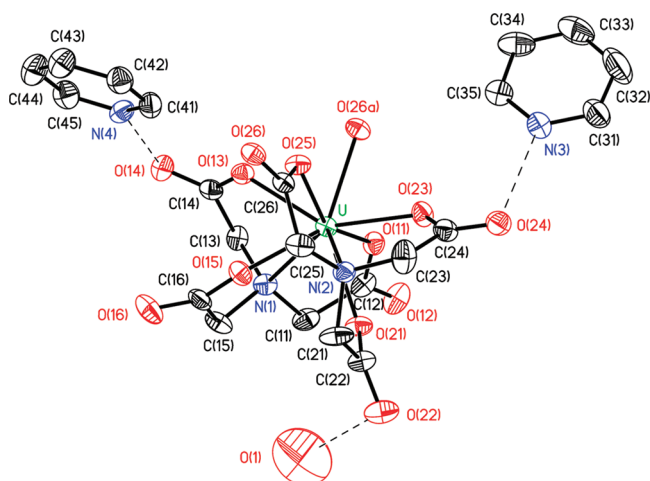
	A				**B**				**C**			
	[An(NTA)$_2$]$^{2-}$				[An(NTA)$_2$]$^{2-}$				[An(NTA)$_2$(H$_2$O)]$^{2-}$			
	S_6 symmetry				C_2 symmetry				C_2 symmetry			
	Th^{IV}	U^{IV}	Np^{IV}	Pu^{IV}	Th^{IV}	U^{IV}	Np^{IV}	Pu^{IV}	Th^{IV}	U^{IV}	Np^{IV}	Pu^{IV}
M−O	2.40	2.34	2.33	2.32	2.41	2.31	2.31	2.30	2.40	2.34	2.34	2.34
M−N	2.71	2.67	2.68	2.68	2.77	2.75	2.71	2.74	2.82	2.77	2.76	2.74

Table 4. Calculated Energies of Structures **B** and **C** Relative to **A** (in kJ mol^{-1})

	Th^{IV}	U^{IV}	Np^{IV}	Pu^{IV}
ΔE (**B**)	+7	+8	+31	+36
ΔE (**C**)	−12	+5	+22	+30

difference between **A** and **C** indicates that eight-coordinate cations are more stable in solution for Np(IV) and Pu(IV) (by 22 and 30 kJ mol^{-1}, respectively) and that nine-coordinate cations are slightly more stable for Th(IV) (by 12 kJ mol^{-1}). For U(IV), the energy difference found between eight and nine coordination is small (5 kJ mol^{-1}), and both coordination modes may exist in solution.

3.3. Single-Crystal X-Ray Diffraction Data of Compound 1. A view of the complex solvate **1**·(H$_2$O) is represented in Figure 6, with selected bond lengths and angles in Table 5. The U atom in **1** is nine-coordinate. The two NTA^{3-} anions are tetradentate, being coordinated to the uranium center by the N atom and by one O atom of each of the three carboxylate groups (Figure 6). The N(2) nitrilotriacetate ligand is bridging through the coordination of the O(26) atom onto a U^{4+} ion of a neighboring

[U(NTA)$_2$]$^{2-}$ entity, leading to a 2-D polymer with zigzag anionic chains in the [010] directions (Figure 7). The coordinating environment of the U^{4+} ion is best described as being in a tricapped trigonal prism configuration, with the two N atoms and the O(26a) in the capping positions (Figure 8). The U−O distances, which are varying from 2.327(5) Å to 2.410 (5) Å, the greatest one being U−O(26a), average to 2.37(3) Å and can be compared to the distinct U−O distances reported in a series of U(IV)−carboxylate species due to the different coordination modes of the carboxylate.[39] The mean U−N bond length of 2.69(2) Å is classical and compared well to those reported in the amido compounds [U(N{CH$_2$CH$_2$NSiMe$_2$^{t}Bu)$_3$X] (X = Cl, Br, I, NEt$_2$) which vary in the 2.67(2)−2.710(5) Å range.[40]

The pyridinium cations and the noncoordinating water molecule act as proton donors in H bonds where proton acceptors are terminal O atoms of nitrilotriacetate anions (Figure 6, Table 6). The arrangement of nitrilotriacetate
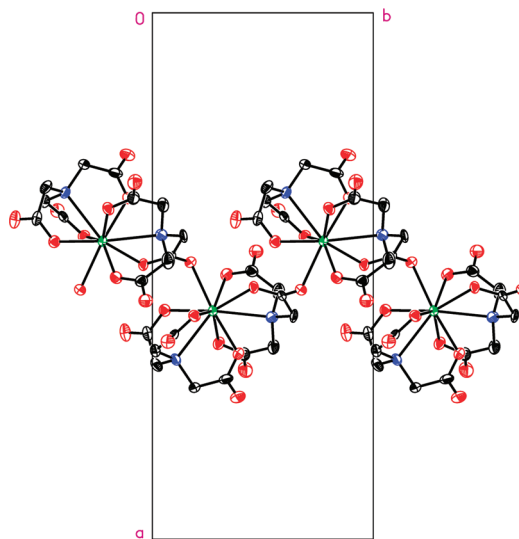

Figure 7. Anionic chain in **1**.

Figure 6. A view of **1** showing the atom-labeling scheme. Displacement ellipsoids are drawn at the 50% probability level. H atoms are omitted. Dashed lines indicate the H-bonding interactions.

Table 5. Selected Bond Lengths (Å) in **1**

U−O(11)	2.327(5)
U−O(13)	2.392(5)
U−O(15)	2.354(5)
U−O(21)	2.365(5)
U−O(23)	2.333(5)
U−O(25)	2.405(5)
U−O(26a)^a	2.410(5)
U−N(1)	2.668(6)
U−N(2)	2.716(7)

^{a} Symmetry transformation for O(26a): ($-x + 1$, $y - 1/2$, $-z + 1/2$).

Figure 8. Coordination polyhedron of the U^{4+} ion in the structure of **1**.

Table 6. H-Bonding Geometry (Å, deg) in **1**

D—H···A	D—H	H···A	D···A	∠D—H···A
N(3)—H(3)···O(24)	0.88	1.82	2.694(10)	173.0
N(4)—H(4)···O(14)	0.88	1.82	2.685(9)	165.6
O(1)···O(22)			2.76(2)	

anions around the U atom, in **1**, is similar to that found in the structure of K$_3$[Er(NTA)$_2$(H$_2$O)]·5H$_2$O.[12] The main difference is that, in the erbium complex, the water molecule is coordinated to the metal center. Thus, we can hypothesized that replacement of the O(26a) atom in **1** supplies a reasonable model of [U(NTA)$_2$(H$_2$O)]$^{2-}$ in aqueous solution.

3.4. EXAFS Data Analysis. EXAFS spectra at the actinide L$_{III}$ edge have been recorded in order to characterize the actinide coordination sphere in aqueous media. We propose here, in comparison with a traditional one-shell fit described below, to use a parametrization of the data adjustment based on the quantum chemical model cluster **A**.

Best fit EXAFS parameters obtained from the one-shell fitting procedure are summarized in Table 7, and both experimental and adjusted EXAFS spectra are presented in Figure 9. Given the usual uncertainty associated with the amplitude values in EXAFS (S_0^2 times N), the number of neighbors has not been fitted and has been arbitrarily fixed to 6, the number of oxygen atoms in model cluster **A** obtained by quantum chemistry (6 or 7 depending on the presence or not of one water molecule in the first coordination sphere). The presence of one water molecule in the cation first coordination sphere (which contributes to roughly 10% of the first shell total amplitude) is insignificant from the EXAFS point of view, given the uncertainty usually associated with amplitude adjustment (between 15 and 20% at best). According to model cluster **A**, the two nitrogen atoms of the NTA ligands are about 0.3 Å further away from the cation than the oxygen atoms of the carboxylate groups are. Given this typical difference in distances, the relative amplitude weight of the two nitrogen atoms to the cation first coordination sphere (about 20%), and the similarity of the backscattering phases and amplitudes between oxygen and nitrogen, the presence of a weak beating node in the EXAFS spectrum should appear around 16 Å^{-1}. This value is far beyond the experimental resolution (11 Å^{-1}). Therefore, according to the geometry of the model clusters, the two nitrogen atoms coming from the two NTA ligands should not contribute significantly to the EXAFS signal of the first coordination shell. Indeed, attempts to add a contribution of two nitrogen atoms as a second shell in the fits presented in Table 7 did not significantly improve the fit quality. In similar systems, some authors have attempted to include the nitrogen contribution as a separate shell, but no estimate of their weight to the total fit is provided.[18] Our results are consistent with a cation polyhedron with only six oxygen atoms from the carboxylate functions directly in the first coordination sphere (with or without an additional water molecule). Accordingly, one can conclude from Table 7 that the average first shell size decreases from 2.39 to 2.32 Å from Th to Pu, in agreement with the well-known actinidic contraction usually observed in coordination chemistry. Finally, one can note from Table 7 that the Debye−Waller values increase

from Th to Pu. This could be consistent with an increase of the shell dispersion or asymmetry (a deviation from the Gaussian shape modeled by Debye−Waller factors) that could be explained by a slight distortion of the cation polyhedron when its size decreases, that is, from Th to Pu. In an attempt to better understand the role of the two nitrogen atoms in the coordination sphere from the beginning to the end of this chemical series, a multishell fitting approach using the parametrized fitting procedure described in the Experimental Section has been undertaken. This fitting procedure has been applied to the Th and Pu complexes, for which the difference in coordination spheres is expected to be most significant. As for the single shell fit, model cluster **A** has been used as a starting model with no water molecules in the first coordination sphere. Best fit parameters are summarized in Table 7 (numbers in italics were fixed or linked, $u = -0.001$, $v = 0.002$, and $w = -0.003$ for the Th complex; $u = -0.005$, $v = 0.004$, and $w = 0.004$ for the Pu complex). In the fit, inclusion of the scattering paths involving the two nitrogen atoms and the two types of carbon atoms of the NTA ligand improves the adjustment between 1.0 and 3.5 Å (not phase-shift-corrected). Both Th−O and Pu−O distances are comparable to that obtained with the one-shell fit, within 0.02 Å, confirming that the two nitrogen atoms were not interfering in the one-shell fit. The Debye−Waller factors associated with the nitrogen shell are abnormally large (the value and uncertainty for Th suggests that the nitrogen shell is indeed insignificant), suggesting again that this shell does not contribute much to the fit. Interestingly, the value is divided by three from Th to Pu, suggesting that both nitrogen atoms are more significant in the plutonium fit than in the thorium one. Removal of the two nitrogen atoms in the adjustment model, everything being kept identical, led to a larger degradation of the r factor for Pu (6.3% instead of 3.9%) versus that for Th (7.1% instead of 6.4%). In conclusion, we suggest that the actinide polyhedron is in a $(6 + 2)_{NTA}$ or $1_{wat} + (6 + 2)_{NTA}$ configuration. In addition, one can note from Th to Pu that (i) the increase in the one-shell fit of the Debye−Waller factor, (ii) the decrease in the parametrized fit of the Debye−Waller factor of the nitrogen shell, and (iii) the increased improvement of the fit quality by inclusion in the parametrized fit of the nitrogen shell suggest an increase of the polyhedron distortion as the atomic number increases. Such assessment should however be tempered by the difficulty of EXAFS itself to be significantly sensitive to the two extra atoms given the overall configuration of the cation coordination sphere.

4. Discussion

The reported set of stability constants corresponding to the formation of 1:1 and 1:2 complexes are consistent along the An(IV) series with decreasing values in the order Th < U < Np < Pu (see Figure 10). The log K_1 and log K_2 values measured for Np(IV) are in good agreement with those reported in the literature[5] (they differ by 0.8 and 0.6 units, respectively). Those constants have also been calculated, taking into account the effect of initial complexation with nitrate and chloride ions (section 2). This effect is weak in

Table 7. EXAFS Best Fit Structural Parameters Obtained Using Both One Shell and Parameterized Fitting Procedures and Single Scattering Approach[a]

sample	distances/Debye−Waller factors	global amplitude factor S_0^2/energy shift factor e_0; ε, $\Delta\chi_\nu^2$, r_factor (%)
Th(IV)/NTA *one shell fit*	*6 O,N* at 2.39(1) Å/σ^2 = 0.0052(8) Å^2	1.0/3.8 0.0042, 0.6, 8.3%
Th(IV)/NTA *parameterized fit*	*6 O* at 2.40(1) Å/σ^2 = 0.0048(5) Å^2 *2 N* at 2.76 Å/σ^2 = 0.0413(400) Å^2	0.9/5.5 0.0042, 0.5, 6.4%
U(IV)/NTA	*6 O,N* at 2.33(1) Å/σ^2 = 0.0053(8) Å^2	0.9/1.9 0.0045, 0.5, 7.9%
Np(IV)/NTA	*6 O,N* at 2.33 Å/σ^2 = 0.0066(9) Å^2	1.1/2.4 0.0039, 0.9, 8.9%
Pu(IV)/NTA	*6 O,N* at 2.32(1) Å/σ^2 = 0.0087(10) Å^2	1.3/0.5 0.0043, 0.6, 9.7%
Pu(IV)/NTA *parameterized fit*	*6 O* at 2.34(1) Å/σ^2 = 0.0096(6) Å^2 *2 N* at 2.69 Å/σ^2 = 0.0124(48) Å^2	1.4/3.6 0.0043, 0.3, 3.9%

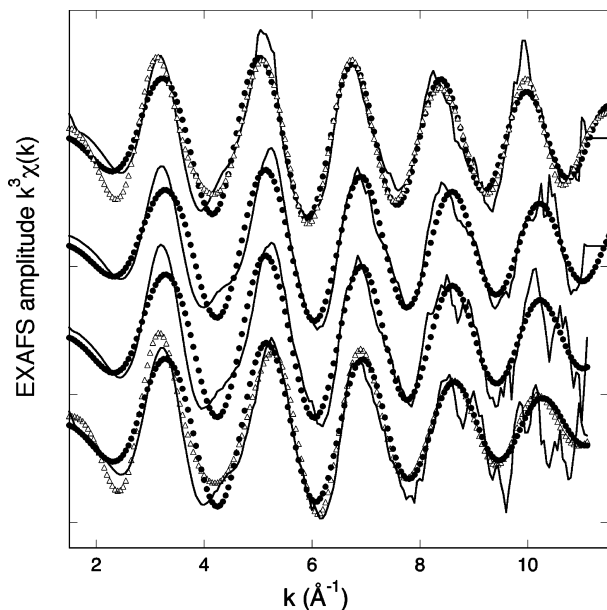[a] Parameters in italics have been fixed or imposed by geometrical constraints.

Figure 9. Experimental (straight line) and best fit (dots and triangles) of the EXAFS spectra of (from top to bottom): Th(IV)/NTA, U(IV)/NTA, Np(IV)/NTA, and Pu(IV)/NTA. Dots = one-shell fit; triangles = parametrized fit.
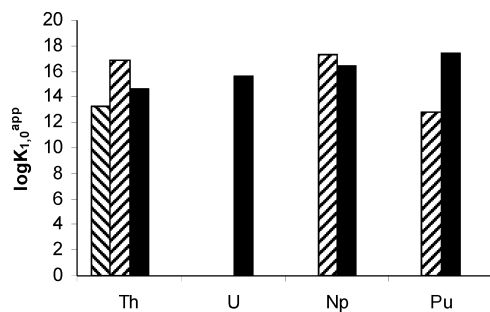

Figure 10. Apparent stability constants of An(IV) complexes (stoichiometry 1:1) with NTA: (black) this work; (shaded, \\\\) [3]; (shaded, ///) [4] (Th), [5] (Np), and [6] (Pu).

comparison with the complexation with NTA and can be neglected in the framework of this study. For Pu(IV), the value of the first stability constant is not in accordance with the literature;[6] our value for log K_1 is higher by more than four units than the one reported. However, the experimental conditions used in the study of Nitsche and Becraft, especially a rather high pH of 1.1, suggest that the disproportionation of Pu^{IV} might have occurred before the measurements. Moreover, the molar extinction coefficient cal-

culated from their spectrum of free Pu is quite higher than what is usually reported for a perchloric medium.[41] In the study of Np(IV)/Th(IV) competition for the complexation with NTA, the deconvolution of the samples' spectra leads to a determination of the apparent formation constant of Th^{IV}L: log K_1 = 14.6 (Table 2). This value is a little higher than expected from our assumptions (log K_1 = 13.25[3]) but is on the same order of magnitude. The value log K_1 = 16.9, found in the literature,[4] seems to be overestimated.

The structural studies performed on the formation of the 1:2 complexes indicate that the carboxylic oxygen atoms are strongly bound to the actinide cation with actinide−oxygen bond distances between 2.3 and 2.4 Å. The nitrogen atoms of the amine are also interacting with the metal center with An−N distances which are comprised between 2.7 and 2.8 Å and which are in the classical range of known U(IV)−N distances.[42] In conclusion, the coordination mode of NTA is tetradentate with three strong actinide−oxygen bonds and one actinide−N interaction.

Note the remarkable agreement between the uranium−oxygen bond distances obtained from EXAFS and quantum chemistry calculations: the average of the six U−O(NTA) distances is equal to 2.34 and 2.33 Å in the calculated and EXAFS structures, respectively. These values agree also very well with the solid-state structure (2.3 Å), although the binding mode of NTA differs from that in solution. For Th(IV), Np(IV), and Pu(IV) in solution, the average An−O distances agree within 0.02 Å between EXAFS and calculations. The total number of coordinated atoms is nine in the crystal structure of U(IV). The coordination number is much more difficult to determine in solution. However, according to the calculations, there is a change of coordination number along the series of actinides, the most stable structure being nine-coordinate for Th(IV) and eight-coordinate for Np(IV)

(38) Martell, A. E.; Smith, R. M.; Motekaitis, R. J. *NIST, Critically Selected Stability Constants of Metal Complexes Database*, version 6.0; NIST Standard Reference Data no. 46; NIST: Gaithersburg, MD, 2001.
(39) (a) Calderazzo, F.; Dell Amico, G.; Pasquali, M.; Perego, G. *Inorg. Chem.* **1978**, *17*, 474–479. (b) Brianese, N.; Casellato, U.; Ossola, F.; Porchia, M.; Rossetto, G.; Zanella, P.; Graziani, R. *J. Organomet. Chem.* **1989**, *365*, 223–232. (c) Rebizant, J.; Spirlet, M. R.; Apostolidis, C. A. *Acta Crystallogr.* **1992**, *C48*, 452–454.
(40) Roussel, P.; Alcock, N. W.; Boaretto, R.; Kingsley, A. J.; Munslow, I. J.; Sanders, C. J.; Scott, P. *Inorg. Chem.* **1999**, *38*, 3651–3656.
(41) Katz, J. J.; Seaborg, G. T.; Morss, L. R. *The Chemistry of the Actinide Elements*; Chapman and Hall: London, 1986; Vol. 1.
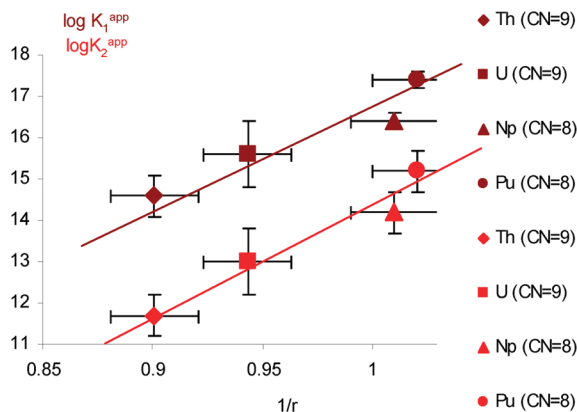(42) Castro-Rodriguez, I.; Olsen, K.; Gantzel, P.; Meyer, K. *J. Am. Chem. Soc.* **2003**, *125*, 4565–4571.

Figure 11. Evolution of the formation constants of An(IV) complexes versus $1/r$, with $CN(Th(IV)) = CN(U(IV)) = 9$ and $CN(Np(IV)) = CN(Pu(IV)) = 8$ (CN = coordination number).

and Pu(IV). When the cation is eight-coordinate, the preferred binding mode according to the DFT calculations corresponds to structure **A** (Figure 5), where the two imino nitrogens are trans to each other.

Stability constants corresponding to the formation of highly charged cations with polyaminocarboxylic ligands are expected to follow roughly a linear trend as a function of the ionic radius. The ionic radius of each cation can be determined for eight- or nine-coordinate cations (r_8 and r_9) from tabulated values, and then, the evolution of the formation constants versus $1/r$ can be plotted for eight- and nine-coordination numbers ($1/r_8$ and $1/r_9$, respectively). In the case of An(IV), if we consider that U(IV), Th(IV), Np(IV), and Pu(IV) are eight-coordinate, the evolution of $\log K$ versus $1/r_8$ is not linear. But if Np(IV) and Pu(IV) are eight-coordinate and Th(IV) and U(IV) are assumed to be nine-coordinate, $\log K$ follows a linear trend (Figure 11). This evolution of the coordination number along the series is in agreement with the DFT calculations.

In the case of 1:2 stoichiometry, the eight-coordinations of Np(IV) and Pu(IV) indicate that four sites of NTA are involved in the formation of the complex, underlining the role of the N atom in addition to the three carboxylate functions as defined by the EXAFS multishell analysis. An additional H_2O molecule could be responsible for the nine-coordination of Th(IV) and probably U(IV).

5. Conclusion

The present study on the coordination of NTA onto An^{4+} cations involved several analytical and simulation techniques, leading to complementary information about the solution and the coordination chemistry of this system. Moreover, comparison of the complex properties across the actinide series led to a better understanding of the coordination behavior of NTA. These data will lead to further interpretation of aminocarboxylate complexation mechanisms in future studies.

Our results suggest the following interpretation. First of all, the coordination number of the cation in the $[An^{4+}](NTA)_2$ complex varies along the actinides series, with CN = 8 for Np(IV) and Pu(IV) and CN = 9 for Th(IV) and probably U(IV), which may indicate the presence of a further water molecule in the first coordination sphere. This interpretation is in agreement with the evolution of the stability constants as well as with the results of DFT calculations. From a structural point of view, the nitrogen atom of NTA is poorly coordinated; however in solution, the cation polyhedron seems to become slightly more distorted from Th to Pu, as demonstrated by the EXAFS data. In the solid state, the coordinating environment of uranium can be best described as a distorted tricapped trigonal prism with both N atoms occupying two capping positions, the third capping position being occupied by an O atom of the bridging nitrilotriacetate anion. In that case, the NTA ligand is best described as a 3 + 1 chelate, depending on the cation involved.

Supporting Information Available: Structure of NTA, stability constants, and additional references. This material is available free of charge via the Internet at http://pubs.acs.org.

IC801453W